Alternative usage of miRNA-biogenesis co-factors in plants at low temperatures

Delfina A. Ré[1,4], Patricia L.M. Lang[1,2,4], Cristian Yones[3], Agustin L. Arce[1], Georgina Stegmayer[3], Diego Milone[3], Pablo A. Manavella[1,*]

[1]Instituto de Agrobiotecnología del Litoral (CONICET-UNL), Facultad de Bioquímica y Ciencias Biológicas, Universidad Nacional del Litoral, 3000, Santa Fe, Argentina.
[2]Max Planck Institute for Developmental Biology, Tübingen, Germany.
[3]sinc(i), Research Institute for Signals, Systems and Computational Intelligence (CONICET-UNL), Ciudad Universitaria, Santa Fe, Argentina.
[4]Equal contribution

Running title: Low-temperature miRNA-biogenesis

Summary statement: Upon a decrease in ambient temperature, the plant miRNA biogenesis machinery produces miRNAs, even in the absence of the key DICER LIKE1 co-factors HYPONASTIC LEAVES 1 and SERRATE.

Keywords: microRNA, Arabidopsis thaliana, temperature, microRNA biogenesis, HYL1

***Corresponding author**
Pablo A. Manavella
Instituto de Agrobiotecnología del Litoral (CONICET-UNL), Facultad de Bioquímica y Ciencias Biológicas, Universidad Nacional del Litoral, 3000, Santa Fe, Argentina
E-mail: pablomanavella@ial.santafe-conicet.gov.ar
Tel: +54 342 4511370 ext. 5013

Abstract

Plants use molecular mechanisms to sense temperatures, trigger quick adaptive responses, and thereby cope with environmental changes. MicroRNAs (miRNAs) are key regulators of plants' development under such conditions. The catalytic action of DICER LIKE 1 (DCL1), in conjunction with HYPONASTIC LEAVES 1 (HYL1) and SERRATE (SE), produces miRNAs from double-stranded RNAs. As plants lack a stable internal temperature to which enzymatic reactions could be optimized during evolution, reactions like miRNA processing, have to be adjusted to fluctuating environmental temperatures.

Here, we report that with decreasing ambient temperature, the plant miRNA biogenesis machinery becomes more robust, producing miRNAs even in the absence of the key DCL1 co-factors HYL1 and SE. This reduces the morphological and reproductive defects of *se* and *hyl1* mutants, restoring seed production. With small RNA sequencing and bioinformatics analyses we identified specific miRNAs whose production becomes HYL1/SE independent in response to temperature decrease, and found that the secondary structure of primary miRNAs is key for this temperature recovery. This finding may have evolutionary implications as a potential adaptation-driving mechanism to a changing climate.

Introduction

In nature, animals can migrate or modify their behavior in response to changes in the environmental temperature. Plants, as sessile organisms, do not have this possibility. With a few exceptions, such as the eastern skunk cabbage (Ito et al. 2004), plants are not thermogenic organisms, and thus lack a homogeneous and stable internal temperature to which biochemical reactions can be optimized during evolution. Instead, most molecular and enzymatic reactions in plants have to be adjusted to the fluctuating environmental temperatures surrounding the plant. Molecular mechanisms that sense temperature, allowing quick adaptive responses, are actively studied. PHYTOCHROME B, for example, was recently described as a main sensor of temperature and light (Jung et al. 2016; Legris et al. 2016). Morphological changes, coordinated by molecular responses, help plants to cope with environmental changes. *Arabidopsis thaliana*, for instance, is well-known to display differential growth patterns when cultivated at different temperatures (Quint et al. 2016). Key regulators of such temperature-sensitive changes in plant development are microRNAs (miRNAs), 21 to 23 nucleotide long, single-stranded RNAs that regulate mRNA transcript abundance (and translation) via sequence complementarity (Liu et al. 2018). Abundance and activity of miRNAs themselves, in turn, is regulated at multiple levels and by fine-tuning elements within the miRNA biogenesis machinery.

Under regular growth chamber conditions (22-23 °C, long-day photoperiod) miRNAs are produced by the catalytic action of the type III ribonuclease DICER LIKE 1 (DCL1). During this reaction, HYPONASTIC LEAVES 1 (HYL1) and SERRATE (SE) are necessary for accurate excision of the mature miRNAs from their long and complex primary transcripts (pri-miRNAs). Mutations in the genes that encode these proteins have severe consequences for miRNA production, stability, homeostasis, and ultimately for plant phenotypic traits (Achkar et al., 2016). Here, we report that upon a decrease in ambient temperature, the plant miRNA biogenesis machinery seems to become more robust and produces miRNAs even in the absence of the key DCL1 co-factors HYL1 and SERRATE. This restored miRNA production reduces the morphological and reproductive defects of mutations in these cofactors, leading to restored seed production. RNAseq analysis, followed by a novel character-extraction protocol applied

to pri-miRNA sequences points towards the secondary structure of pri-miRNAs as one of the main features enabling miRNA processing at low temperatures despite a lack of (at normal temperatures crucial) co-factor activity.

Results and Discussion

Low temperatures increase miRNA-biogenesis mutant fitness and miRNA production

A. thaliana plants with mutations in miRNA biogenesis cofactor-coding genes like *HYL1* or *SE* normally display strong developmental defects and low seed production when grown in standard chamber conditions (long day conditions (LD) 23 °C, (Rogers & Chen 2013)). However, when cultivated at 16 °C, the same mutant lines perform better and show an overall attenuated phenotype (Fig. 1). Rosette size, leave shape and flower development in *hyl1-2* and *se-3* mutants resemble the wild-type phenotype more when grown at 16 °C than at 23 °C (Fig. 1A and S1A-B). This is paralleled by restored seed production, a reduced embryonic abortion and increased pollen viability (Fig. 1B-E and S1C). This effect of lower temperature is however not evidenced in mutants affecting proteins downstream of the core miRNA-biogenesis machinery, and hence downstream of DCL1, HYL1 and SE, such as *ago1-25* and *hen1-5* (Fig. 1 and S1A), suggesting that the effects caused by lowering the temperature occur during the initial steps of miRNA biogenesis.

To assess whether the increase in plant fitness was related to higher miRNA production at low temperature, we used small RNA blots to quantify miRNAs. We observed that the production of several miRNAs in *hyl1-2* and *se-3* mutants grown at 16°C was restored to almost wild-type levels (Fig. 2A). In contrast, in *ago1-25* mutants, temperature did not affect miRNA levels (Fig. 2B), which is consistent with the hypothesis that temperature affects mainly the initial steps of miRNA biogenesis and processing. Notoriously, *hen1-5* mutants present an increment in miRNA accumulation at 30 °C (Fig. 2B). Most miRNAs, with a few exceptions, did not show an increased accumulation at 16 °C in Col-0. This could perfectly reflect that in wild-type plants, where the miRNA machinery is fully active, pri-miRNAs are processed equally well at both temperatures, reaching a potential maximum of miRNA production set by the

amount of pri-miRNA transcribed. A few miRNAs, miR173, miR161 and miR172, showed decreased levels at 30°C in Col-0 plants which may reflect differential regulation (Fig. 2A and B). The last mentioned experiments were performed using plants grown at the indicated temperatures for 5 days. To discard effects caused by the delayed development expected for plants cultivated at lower temperatures, we grew Col-0 and *hyl1-2* plants for 5 days at 23 °C and then transferred them to 16 °C for variable periods of time, and vice versa. We then quantified several miRNAs with small RNA blots and observed that lowering the environmental temperature (i.e. transfer from 23 °C to 16 °C) led to an increase of miRNA accumulation in *hyl1-2* and *se-3*, even after short exposure to lower temperature (6 to 24 hs, Fig. 2C, D). These kinetics were not mirrored by a similarly fast decrease in miRNA levels in plants grown at 16 °C and transferred to 23 °C. Here, it took almost 4 days to see the decrease in miRNAs, possibly due to a slower turnover of already produced miRNAs (Fig. 2C). Interestingly, miR157 showed a reduction in Col-0 after 24 hours of being transferred to 16 °C, prior to increasing above initial concentrations, which may reflect a complex transcriptional regulation of this miRNA in this condition (Fig. 2D). Moreover, RNA sequencing analysis showed that the observed increase in miRNA levels at low temperature could not be explained by increased miRNA transcription, as the expression of pri-miRNAs between samples cultivated at different temperatures was stable and did not recapitulate the observed miRNA dynamics (Table S1). This analysis was confirmed using *MIRNA* promoters fused to the reporter gene *GUS*. Plants transformed with these constructs were grown at 16 °C or 23 °C and the promoter activity was assayed by histochemical staining, showing unchanged promoter activity, and hence that the tested *MIRNAs'* transcription was not increased at 16 °C (Fig. 3A). This supported the notion that it is the enhanced processing of pri-miRNAs at 16 °C, even in the absence of the co-factors, rather than increased transcription of miRNA genes, that leads to the observed mutant phenotype rescue. Interestingly, the time required to observe a clear temperature effect on miRNA accumulation varies depending on the miRNA; for example, the increment of *miR164* and *miR167* is observed after 6 hs at 16 °C (Fig. 2D), while for *miR161* and *miR156,* 24 hs are necessary (Fig. 2C). These differences might be related to the transcription rate of each miRNA. However, this observation may also suggest that the

miRNA production recovery depends on the nature of the complex and highly variable miRNA precursor and its secondary structure.

Pri-miRNA pairing energy of the secondary structure defines miRNA HYL1 dependence

The fact that the observed temperature-dependent miRNA recovery was similar both in *hyl1-2* and *se-3* mutants suggests that the lower temperature may enhance miRNA processing itself, rather than inducing the expression of potential redundant, homologous factors. While SE does not have close homologs in Arabidopsis, the HYL1 protein family has five members that can potentially act redundantly. We evaluated this possibility by quantifying the transcript levels of HYL1's closest homologs, *DRB2, DRB3, DRB4* and *DRB5* in Col-0 and *hyl1-2* plants grown at 16 °C and 23 °C, using RNA sequencing. The expression of none of these genes was induced by cold neither in the WT nor the *hyl1-2* background, which would have been an expectation if any of these homologs were helping to balance the lack of functional HYL1 in the *hyl1-2* background at low temperature (Table S1). To further confirm this, we obtained *hyl1-2/drb2, hyl1-2/drb3, hyl1-2/drb4* and *hyl1-2/drb5* double mutants and measured miRNA levels in plants grown at both 16 °C and 23 °C (Fig. 3B). The miRNA accumulation in all tested double mutants mirrored that of the *hyl1-2* single mutant (Fig. 3B), dismissing a potential redundancy effect triggered by temperature as causal for the observed attenuated phenotypes.

Additionally, RNAseq analysis comparing the transcriptome of Col-0 and *hyl1-2* plants grown at 16 °C or 23 °C also did not identify any plausible non-homolog candidate to compensate HYL1 deficiency at low temperature (Table S1). We found 492 significantly differentially expressed genes (q-value < 0.05) in *hyl1-2* mutants grown at 23 compared to 16°C, 365 of them exclusive to the *hyl1-2* background and not affected in Col-0 plants treated in the same way (Fig. 3C, Table S1). If any factor would be taking over HYL1 functions at 16 °C in the *hyl1-2* mutant background, it could be expected to be found among the 302 genes higher expressed at 16 °C in *hyl1-2* plants (i.e. appearing downregulated in *hyl1-2* at 23 °C, see Fig. 3C orange balloon). A gene ontology analysis showed that among those genes, only 37 have DNA or RNA binding properties, but the majority belongs to transcription factor families, proteins related to

DNA damage repair or translation initiation factors (Table S1), which are unlikely to display HYL1-like properties or activity. Further, when specifically tested, no miRNA-biogenesis related factors appeared differentially regulated among these temperatures (Table S1).

In addition, we observed that the production of some miRNAs was not restored by a temperature reduction (i.e., miR157) or not affected in *hyl1-2* mutants independent of the temperature (i.e., miR168) (Fig. 2A, C). Aiming to sort miRNAs into categories, we performed small RNA sequencing of Col-0 and *hyl1-2* plants grown at 23 °C and 16 °C. We then categorized miRNAs according to their responsiveness to temperature changes into two groups: i) those with increased expression in *hyl1-2* when temperature changed from 23 to 16ºC (TC), and ii) those that did not increase their expression with the temperature variation (TnC) (Fig. 3D). It is worth mentioning that, due to the identical sequence of some mature miRNAs that belong to the same family, some miRNAs may be wrongly categorized if a single member of the family "hides" the others (e.g. a temperature responsive member of a family among non-responsive ones). This can potentially reduce the power of our analysis.

Based on the miRNA-group sorting, we aimed to evaluate if structural or sequence characteristics of the corresponding pri-miRNAs can help define how a miRNA responds to temperature, and to what extent its processing is HYL1 dependent. For this, 1,590 pri-miRNA features were extracted from each group using miRNAfe (Yones et al. 2015), a feature selection method based on LASSO (Table S2, (Zou & Hastie 2005). In our analysis, a positive LASSO coefficient for a feature indicates that the feature is important for the temperature responsiveness (TC), while a negative coefficient indicates that the feature is important for the temperature non-responsiveness (TnC). We found that the most important features of miRNAs that increase expression in *hyl1-2* background at 16 ºC are the presence and amount of GCA and UGCA (Fig. 3E). Interestingly, the content of paired G or C nucleotide triplets in the pri-miRNA structure appeared top ranked. This suggests that such high energy paired regions of the pri-miRNA are a defining feature for HYL1-dependency during pri-miRNA processing. As temperature change will affect the folding and secondary structure of pri-miRNAs, features highly dependent on the GC content of the paired region are particularly relevant. In our analysis, other characteristics such as the

number of loops or loop size were not found to be relevant for the classification (Table S2). However, a comparison between our pri-miRNA classification and the DCL1-slicing mechanism (Bologna et al. 2013; Chorostecki et al. 2017) showed that HYL1-independent miRNAs tend to be processed via a short base-to-loop mechanism by DCL1 (Table S3). This correlation may indicate that proper pri-miRNA slicing by DCL1 can be independent of HYL1 for short base-to-loop processed precursors, while HYL1 becomes necessary to guide DCL1 when multiple slicing steps are required in long, complex pri-miRNAs, or when slicing starts from a less organized loop region.

A drop in temperature improves the miRNA processing precision

Help of SE and HYL1 to DCL1 during miRNA processing has been shown to be essential to ensure the ribonuclease precision at the mature miRNA excision step (Dong et al. 2008; Liu et al. 2012). Given our results, it could be expected that a change in pre-miRNA stability/folding triggered by a drop in temperature could improve miRNA processing precision. We therefore analyzed processing precision by scoring the ratio of total miRNA-matched small RNA to the pool of imprecisely processed small RNAs, defined as those only partially matching the mature miRNA sequence. As reported, hyl1-2 mutants grown at 23 ºC showed a drastic reduction in processing precision when compared to Col-0 at the same temperature (Fig. 4A). However, reduction in temperature drastically improved miRNA-processing precision. This is particularly true in *hyl1-2* mutants, as could be anticipated from our previous results, but also for wild-type plants, which display increased precision upon temperature decrease (Fig. 4A). This suggests overall increased robustness of the processing machinery at 16 ºC, coinciding with increased thermodynamic stability of pri-miRNA secondary structure.

It has been recently shown that the pool of active HYL1 is actively degraded when plants are exposed to insufficient light for a prolonged period (Achkar et al. 2018). Light reduction in the shade, or complete darkness, are often accompanied by a drop in temperature. We wondered how such temperature changes could affect HYL1-dependent miRNA processing when HYL1 is degraded simultaneously. To test a combined scenario of low temperature and insufficient light, we sequenced small RNAs of plants grown at 16 or 23 ºC in LD photoperiod for 14 days, or grown for 10 days in LD and then transferred to dark for 4 days, and compared the miRNA accumulation (Fig.

4B). As previously reported, we observed an overall reduced miRNAs accumulation when the plants were transferred to the dark, as consequence of HYL1 degradation, but also a partial recovery of the miRNA populations when the plants were kept at 16 ºC (Fig. 4B). Additionally, a processing precision analysis performed in these samples showed increased processing precision in Col-0 plants when the temperature drops, even in the absence of light (Fig. 4C), a result harmonious with our hypothesis.

Closing remarks

Our results demonstrate that some, but not all, miRNAs could go through alternative processing less dependent on DCL1 co-factors when the environmental temperature is below standard growth chambers conditions. Given the extensive distribution of Arabidopsis worldwide and the fact that 16 °C is the average temperature during spring/summer in central Europe, the center of *A. thaliana*'s geographic distribution, our finding gains ecological relevance. Variation in *HYL1* itself seems unlikely to trigger a necessity for alternative processing pathways: In a polymorphism analysis using 309 *Arabidopsis thaliana* accessions from across the plant's natural geographic range (1001 Genomes Consortium 2016), we found very little variation in *HYL1*. We could not detect any polymorphism causing nonsense mutations, and all variants causing non-synonymous mutations fall in the C-terminal end of the protein, which has been reported to be dispensable for HYL1 activity (Fig. 4D, (Wu et al. 2007)). This lack of natural genetic variation affecting HYL1 functionality suggests that HYL1 may be necessary for plant homeostasis even in colder climates.

However, we recently showed that HYL1 protein levels themselves change under certain environmental conditions – prolonged periods of insufficient light induce HYL1 degradation (Achkar et al. 2018). Since darkness or shading, common and highly relevant ecological conditions, often coincide with a drop in temperature, the results described here prompt us to envision a complex regulatory mechanism where dark will induce HYL1 degradation, while at the same time the associated temperature drop will turn HYL1 dispensable for the processing of some miRNAs. This implies a versatile and environmental dependent miRNA biogenesis pathway that allows the production of subsets of miRNAs under given conditions. This gives the miRNA biogenesis pathway,

once believed to be ubiquitous and constant, large flexibility to produce subsets of miRNAs. Finally, the finding that such a temperature recovery of miRNA production is ruled by the secondary structure of the pri-miRNAs may have significant evolutionary implications as a potential adaptation-driving mechanism.

Materials and Methods

Plant Material

Arabidopsis thaliana Columbia (Col-0, wild type / WT) seeds were surface sterilized with 10 % (v/v) bleach and 0.5 % SDS and stratified for 2–3 days at 4 °C. Plants were grown at indicated temperatures, for the indicated time periods, on soil or MS-Agar plates in long day conditions (16 h light: 8 h dark), in ARALAB D1200 PL growing chambers (ARALAB, Portugal). Temperature fluctuations > 1 °C could buffer the observed effect on miRNA production in the plants. Thus in all cases, the incubator temperature was set up to oscillate in a range < to +/- 1 °C and temperature was monitored during the whole duration of the experiments. Mutant lines were obtained from ABRC or NASC stock centers: *drb2* (N349415), *drb3* (SALK_022644C), *drb4* (SALK_000736), *drb5* (SALK_126609.29.25.N), *hen1-5* (SALK_049197), *hyl1-2* (SALK_064863), *se-3* (Grigg et al. 2005) and *ago1-25* (Morel et al. 2002).

RNA Analysis

Total RNA was extracted using TRIZOL reagent (Life Technologies). RNA blots were made as previously described (Tomassi et al. 2017). Briefly, 1-5 µg of total RNA were resolved in 17 % (v/v) polyacrylamide gels under denaturing conditions (7 M urea) and then transferred to HyBond-N+ charged nylon membranes (Amersham) by semi-dry electroblotting. RNA was covalently fixed to membranes using a UV Crosslinker. Membranes were hybridized over-night with DNA oligonucleotide probes labeled with the second generation DIG Oligonucleotide 3'-End Labeling Kit (Roche); the signal was detected using CSPD ready-to-use solution (Roche), by exposure to Amersham hyperfilm ECL (GE Healthcare Life Sciences). See Table S4 for probe details.

RNA Sequencing

Small RNA libraries were prepared as indicated by the TruSeq small RNA library prep kit (Illumina). 50 ng of small RNAs purified with the ZR small-RNA PAGE Recovery Kit (Zymo Research) were used as input for library preparation. RNA libraries were prepared using 1 ug of total RNA as input, as described by the TruSeq RNA sample prep V2 guide (Illumina). Small RNA and mRNA library size selections were performed with the BluePippin System (SAGE Science) using a 3% and 1.5% gel, respectively. Single-end Illumina sequencing was performed with a HiSeq3000. Obtained sequence data are available at the European Nucleotide Archive (ENA) under the project number PRJEB28610.

MiRNA Classification and Feature Extraction

Small RNA reads were first processed to remove 3´ adapters using cutadapt (version 1.9.1; (Martin 2011) and then mapped using bowtie (version 1.1.2; (Langmead et al. 2009)). The references used for mapping were the databases for hairpin and mature miRNAs for *A. thaliana* from miRBase (release 21), in the latter mature miRNAs with identical sequences were collapsed into single miRNAs. For all the reads from Col-0 and *hyl1-2* plants the log2 fold change (LFC) for each genotype at 16 ºC compared to 23 ºC was calculated with DESeq (Anders & Huber 2010). Reads with LFC<0 and false discovery rate adjusted p-value <0.1 at 23 ºC were discarded. The remaining reads were divided into two groups: i) temperature changing (TC) sequences, with increased expression in hyl1-2 when the temperature changed from 23 to 16 ºC and ii) temperature non-changing (TnC) sequences that did not increase their expression with temperature variation. The median LFC (θ) was used as a threshold for separation into these two groups. This criterion left equal numbers of reads in each group, leaving in TC those with expression levels increased by more than 80 % LFC upon temperature change from 23 to 16 ºC. Feature selection was based on LASSO (Zou & Hastie 2005). The optimization criteria was $L = |LFC - AX\beta|2 + \lambda 2 \sum j \beta j 2 + \lambda 1 \sum j |\beta j|$, where X is the matrix of pre-miRNA features and A has the confidence levels for each sequence. This is a diagonal matrix with elements αi, defined according to the difference between the distance of each sequence i to the threshold θ that separates the two groups (TC and TnC),

and the standard error (SE) in the detection of the miRNA within the sequence. That is, $\alpha i = 2 / (1 + \exp(-5(|LFCi - \theta| - SEi))$, for $|LFCi - \theta| > SEi$; and $\alpha i = 0$ otherwise (the feature is ignored in the optimization). To solve the optimization problem, a grid search was performed over $\lambda 1$ and $\lambda 2$, calculating the optimal β for each combination in a cross-validation scheme. Finally, the combination of $\lambda 1$ and $\lambda 2$ that leads to the lower mean loss is used to estimate the final β (Yones et al. 2015).

Transcriptomic Analysis

The mRNA-seq reads were first filtered by mapping them to the A. thaliana 18s ribosomal RNA with Bowtie2 (version 2.2.6, (Langmead & Salzberg 2012). Unmapped reads were then aligned to the *A. thaliana* genome using Tophat2 (version 2.1.0, (Kim et al. 2013)) with the TAIR10 gene annotation and the following parameters: no-novel-juncs, read-edit-dist 1, read-gap-length 0, max-multihits 1. Finally, differentially expressed genes were found with cuffdiff (version 2.2.1, (Trapnell et al. 2012)) using the default parameters, discarding genes with less than 10 counts and considering differentially regulated genes as those with an FDR adjusted p-value < 0.05.

Pollen Tube Staining and Embryo Analysis

Flowers were fixed (10% acetic acid, 30% chloroform, 60% EtOH; 2h) ~16-24h after pollination, incubated in NaOH (4M; 4-6h) and washed three times (50mM potassium phosphate pH 7.5). After staining with DABS (0.1% (w/v) aniline blue, 108mM K3PO4 pH 11, decolorized overnight at 4 °C in the dark before use; 12h, RT), pistils were imaged at 40X with a stereoscope (Leica MZ10F), using 420 nm excitation and a CFP filter.

To evaluate fertilization and embryo production efficiency, fully elongated and filled, but not fully ripened siliques were opened longitudinally and imaged with a stereoscope (Nikon SMZ800).

Histochemistry

Plants containing MIRNA Promoter:GUS constructs were grown on MS-Agar plates for 8 days at 23 °C in LD conditions, and then transferred to 16 °C or kept at 23 °C for 6

more days until histochemistry assay was performed. GUS activity was detected by immersing whole plants in a 1 mM 5-bromo-4-chloro-3-indolyl-glucuronic acid solution in 100 mM sodium phosphate pH 7.0 and 0.1 % Triton X-100, applying vacuum for 5 min, and subsequent overnight-incubation at 37 °C. Chlorophyll was cleared from the plant tissues by immersing them in 70 % ethanol. Images were taken with a LEICA MZ10F.

Acknowledgements

This work was supported by ANPCyT (Agencia Nacional de Promoción Científica y Tecnológica, Argentina), HFSP (Human Frontier Science Program), the Max Planck Society, ICGEB (International Centre for Genetic Engineering and Biotechnology) to P.A.M.. A short-term fellowship from the DAAD (Deutscher Akademischer Austauschdienst) to P.L.M.L., D.A.R., A.L.A., G.S., D.M., and P.A.M., are members of CONICET; C.Y. is a fellow of the same institution.

Competing interests

The authors declare no competing or financial interests.

Author contributions

Conceptualization and methodology, D.A.R., P.L.M.L., G.S., D.M. and P.A.M.; Investigation, D.A.R., P.L.M.L., A.L.A., and D.Y.; Formal Analysis, A.L.A., G.S., D.Y. and D.A.R.; Supervision, P.A.M., and D.M.; Writing – Original Draft, D.A.R. and P.A.M.; Writing – Review & Editing, all authors.

Data availability

Raw data for RNA and smallRNA sequencing have been deposited in the European Nucleotide Archive (ENA) under the project number PRJEB28610.

Supplementary information

Supplemental Information available online.

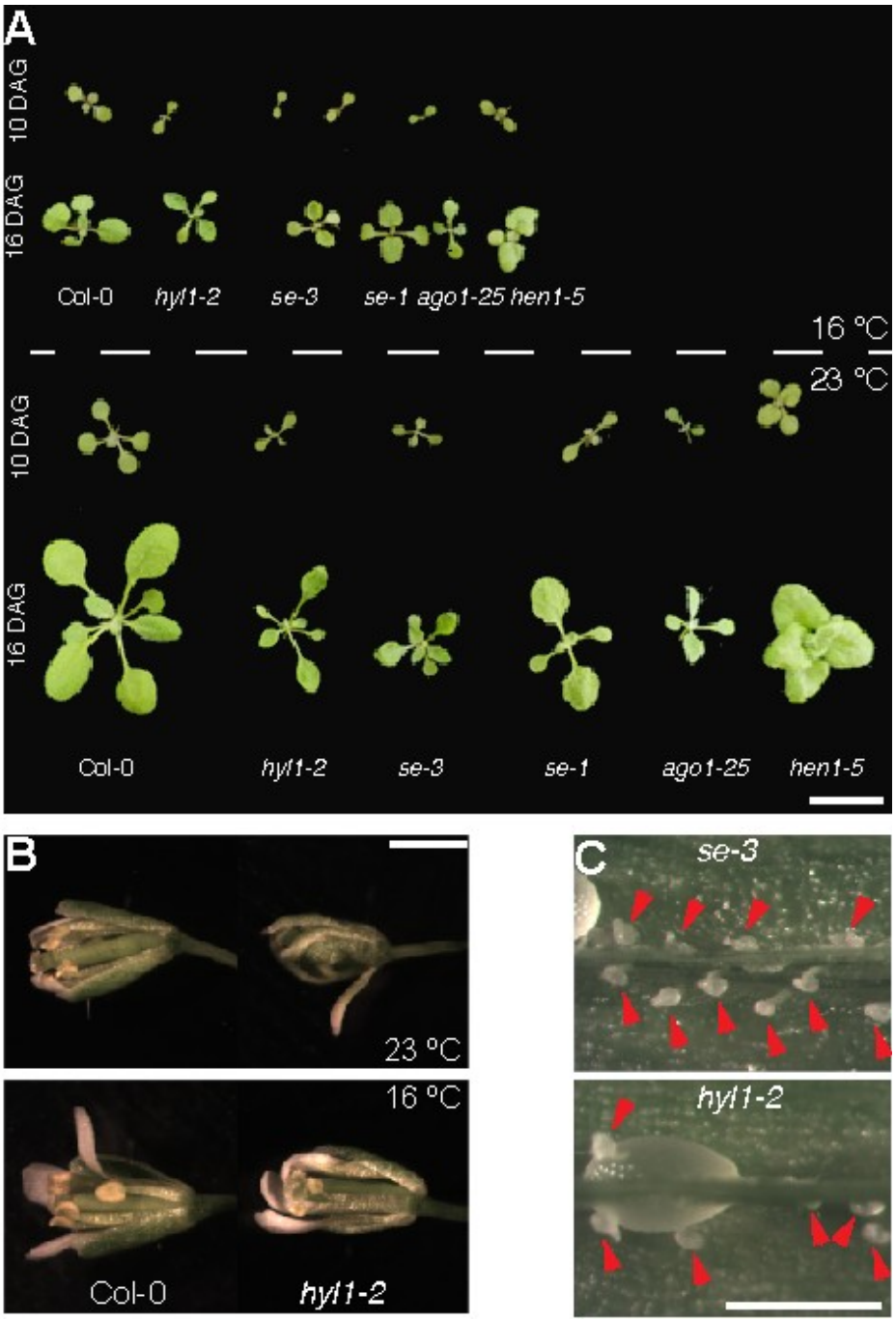

Supplemental Fig. 1: Phenotypes of miRNA biogenesis mutants at reduced temperatures.

Supplemental Table 1: Differentially expressed genes in Col-0 and *hyl1-2* at 16 and 23 °C as shown by RNAseq analysis.

Supplemental Table 2: Differentially accumulated miRNAs in Col-0 and *hyl1-2* at 16 and 23 °C as shown by small RNAseq analysis.

Supplemental Table 3: Pri-miRNA extracted features description.

Feature Name	Description	Dimension
Nucleotide proportion (A, C, G, U)	Ratio of each base in the sequence	4
Dinucleotide proportions per region	Proportion of dinucleotide elements (AA, AC, AG, etc.) in the whole sequence, only in the stem and the main loop	48
Trinucleotide proportion	Similar to the previous feature but combining four bases	192
Tetra-nucleotide proportion	Similar to the previous feature but combining three bases	768
L	Sequence length	1
$G+C_{content}$	Aggregated proportion of guanine and cytosine in the sequence: $G+C_{content}=\frac{G+C}{G+C+A+U}$	1
G/C_{ratio}	Ratio of guanine over cytosine: $G/C_{ratio}=\frac{G}{C}$	1
Ns	Number of stems	1
Avg_BP_Stem	Average number of base pairs per stem	1
Longest stem length	Longest region where the pairing is perfect	1
Terminal loop length	Number of nucleotides in the stem region of the secondary structure	1
Number of base pair	Number of paired nucleotides divided by 2	1
dP or base pair propension	Number of base pair divided by the nucleotide number	1
$\lvert A-U\rvert/L$, $\lvert G-C\rvert/L$, $\lvert G-U\rvert/L$	Number of each possible base pair normalized by the sequence length	3
$\%(A-U)/N_s$, $\%(G-C)/N_s$ and $\%(G-U)/N_s$	Proportion of base pairs on stems	3
Triplets	Vector of 32 elements with the triplets frequency. A triplet is an element formed with the structure composition (paired or not paired) of three adjacent nucleotides and the base at the middle. An example of a triplet is ".((A", where the parenthesis represent a paired nucleotide, a dot a non-paired one, and the letter is the middle nucleotide	32
Tri-triplets	Similar to the triplets, but with three states (pair or unpaired) and three bases. For example: ".(.AGU"	512
MFE	Minimum free energy	1
EFE	Ensemble free energy	1
Freq	The structural frequency calculated with RNAfold (-p option)	1
Diversity	The structural diversity calculated with RNAfold (-p option)	1
Diff	It is |MFE−EFE|/L	1
dG	Minimum free energy divided by the sequence length	1
Adjusted Shannon's entropy or dQ	It characterizes the probability of base pairing in a secondary structure as a chaotic dynamic system: $dQ=\frac{1}{l}\sum p_{ij}\log_2 p_{ij}$, where p_{ij} is the probability of pairing of nucleotides i and j. This value is calculated with the algorithm from (McCaskill, 1990)[1]. Low values of dQ correspond to distributions dominated by a few bases likely to be matched. These bases are better predicted than those that have multiple alternative states	1
MFEI1	Ratio between the minimum free energy and the %C + G	1
MFEI2	Is calculated as dG/Ns, where Nl is the number of stems	1
MFEI4	Is calculated as M F E/Nb , where Nb is the total number of base pairs in the secondary structure	1
max_s	Longest region where the pairing is perfect	1

1 J.S. McCaskill. The equilibrium partition function and base pair binding probabilities for RNA secondary structure. Biopolymers, 29(6-7):1105–1119, 1990

M_b	Number of bulges with length 1, 2, 3 and >4 in the region of the mature on the secondary structure	4
M_{dP}	Base pair propension in the mature region	1
M_{fd}	Distance from the first pair to the mature	1
M_{ld}	Distance from the mature to the main loop	1
M_l	Mature length	1
Total no. of features extracted		1590

Supplemental Table 4: DNA oligonucleotide used as probes.

Supplemental Table 5: Transgene constructs used.

Transgene	Name	Description	Reference
miR171A$_{Prom}$:GUS	pPM181	Genomic DNA of *MIR171A promoter* cloned in pGWB433	Manavella *et al.*, 2013
miR170$_{Prom}$:GUS	pPM203	Genomic DNA of *MIR170 promoter* cloned in pGWB433	Manavella *et al.*, 2013
miR416$_{Prom}$:GUS	pPM409	Genomic DNA of *MIR416 promoter* cloned in pGWB433	This work
miR167A$_{Prom}$:GUS	-	Genomic DNA of *MIR167A promoter* cloned in pBGWFS7	Wu *et al.*, 2006

References

1001 Genomes Consortium, 2016. 1,135 Genomes Reveal the Global Pattern of Polymorphism in Arabidopsis thaliana. *Cell*, 166(2), pp.481–491.

Achkar, N.P. et al., 2018. A Quick HYL1-Dependent Reactivation of MicroRNA Production Is Required for a Proper Developmental Response after Extended Periods of Light Deprivation. *Developmental Cell*, 46(2), pp.236–247.e6.

Anders, S. & Huber, W., 2010. Differential expression analysis for sequence count data. *Genome biology*, 11(10), p.R106.

Bologna, N.G. et al., 2013. Multiple RNA recognition patterns during microRNA biogenesis in plants. *Genome research*, 23(10), pp.1675–1689.

Chorostecki, U. et al., 2017. Evolutionary Footprints Reveal Insights into Plant MicroRNA Biogenesis. *The Plant cell*, 29(6), pp.1248–1261.

Dong, Z., Han, M.-H. & Fedoroff, N., 2008. The RNA-binding proteins HYL1 and SE promote accurate in vitro processing of pri-miRNA by DCL1. *Proceedings of the National Academy of Sciences of the United States of America*, 105(29), pp.9970–9975.

Grigg, S.P. et al., 2005. SERRATE coordinates shoot meristem function and leaf axial patterning in Arabidopsis. *Nature*, 437(7061), pp.1022–1026.

Ito, K. et al., 2004. Temperature-Triggered Periodical Thermogenic Oscillations in Skunk Cabbage (Symplocarpus foetidus). *Plant & cell physiology*, 45(3), pp.257–264.

Jung, J.-H. et al., 2016. Phytochromes function as thermosensors in Arabidopsis. *Science*, 354(6314), pp.886–889.

Kim, D. et al., 2013. TopHat2: accurate alignment of transcriptomes in the presence of insertions, deletions and gene fusions. *Genome biology*, 14(4), p.R36.

Langmead, B. et al., 2009. Ultrafast and memory-efficient alignment of short DNA sequences to the human genome. *Genome biology*, 10(3), p.R25.

Langmead, B. & Salzberg, S.L., 2012. Fast gapped-read alignment with Bowtie 2. *Nature methods*, 9(4), pp.357–359.

Legris, M. et al., 2016. Phytochrome B integrates light and temperature signals in Arabidopsis. *Science*, 354(6314), pp.897–900.

Liu, C., Axtell, M.J. & Fedoroff, N.V., 2012. The helicase and RNaseIIIa domains of Arabidopsis Dicer-Like1 modulate catalytic parameters during microRNA biogenesis. *Plant Physiology*, 159(2), pp.748–758.

Liu, H. et al., 2018. Small but powerful: function of microRNAs in plant development. *Plant cell reports*, 37(3), pp.515–528.

Martin, M., 2011. Cutadapt removes adapter sequences from high-throughput sequencing reads. *EMBnet.journal*, 17(1), p.10.

Morel, J.-B. et al., 2002. Fertile hypomorphic ARGONAUTE (ago1) mutants impaired in post-transcriptional gene silencing and virus resistance. *The Plant cell*, 14(3), pp.629–639.

Quint, M. et al., 2016. Molecular and genetic control of plant thermomorphogenesis. *Nature Plants*, 2(1), p.15190.

Rogers, K. & Chen, X., 2013. Biogenesis, Turnover, and Mode of Action of Plant MicroRNAs. *The Plant cell*, 25(7), pp.2383–2399.

Tomassi, A.H. et al., 2017. Nonradioactive Detection of Small RNAs Using Digoxigenin-Labeled Probes. *Methods in molecular biology* , 1640, pp.199–210.

Trapnell, C. et al., 2012. Differential gene and transcript expression analysis of RNA-seq experiments with TopHat and Cufflinks. *Nature protocols*, 7(3), pp.562–578.

Wu, F. et al., 2007. The N-terminal double-stranded RNA binding domains of Arabidopsis HYPONASTIC LEAVES1 are sufficient for pre-microRNA processing. *The Plant cell*, 19(3), pp.914–925.

Yones, C.A. et al., 2015. miRNAfe: A comprehensive tool for feature extraction in microRNA prediction. *Bio Systems*, 138, pp.1–5.

Zou, H. & Hastie, T., 2005. Regularization and variable selection via the elastic net. *Journal of the Royal Statistical Society. Series B, Statistical Methodology*, 67(2), pp.301–320.

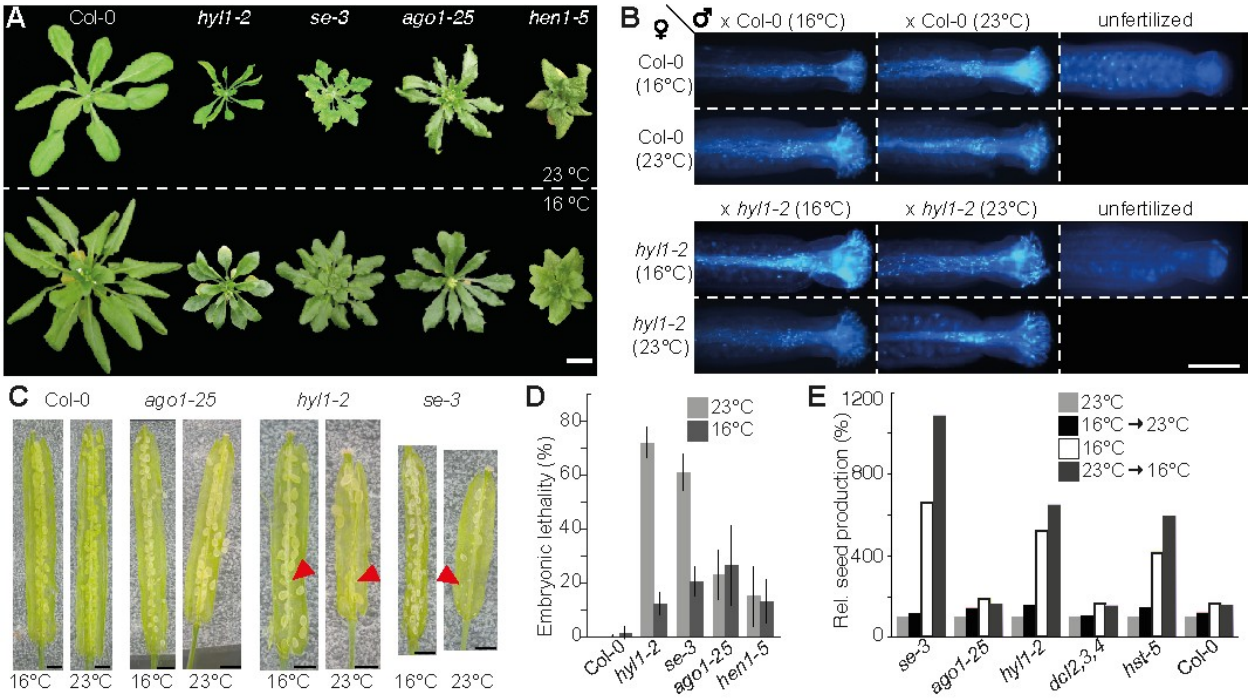

Fig. 1. Reversion of the phenotypes of miRNA biogenesis mutants at reduced temperatures. (A) Phenotypes of wild-type Col-0 and mutants plants at vegetative stage grown at 23 or 16 °C. Scale bar on the bottom right corner represents 1 cm. (B) Col-0 or *hyl1-2* flowers from plants grown at 16 or 23 °C during the reproductive phase artificially pollinated with pollen of plants grown in the same conditions. Sixteen hours after pollination, pollen viability and pollen tube growth were visualized by aniline blue staining. Scale bar in the bottom right corner represents 0.15 mm. (C) Dissection of Col-0 and mutant siliques showing a larger degree of embryonic abortion in *hyl1-2* and *se-3* mutants grown at 23 °C when compared to 16 °C. Examples of aborted embryos are noted with red while a magnification is shown in Fig. S1C. Scale bar in the bottom right corner represents 1 mm. (D) Quantification of the percentage of aborted embryos in WT and mutants plants grown at 23 °C and 16 °C. For each genotype, 50 siliques were dissected and embryo abortion was counted. Embryonic lethality is given as the % of aborted embryos over the total number of embryos. Error bars show 2xSEM. (E) Seed production of different miRNA-related mutants. Plants grown at 23 °C the entire life cycle (light grey), at 16 °C the entire life cycle (white), at 16 °C during vegetative phase and then transferred to 23 °C for the reproductive phase (black bars), or vice versa

(dark grey). The total seed weights of 50 pooled plants are expressed as relative to the seed weights of the same mutants grown at 23 °C the entire lifecycle.

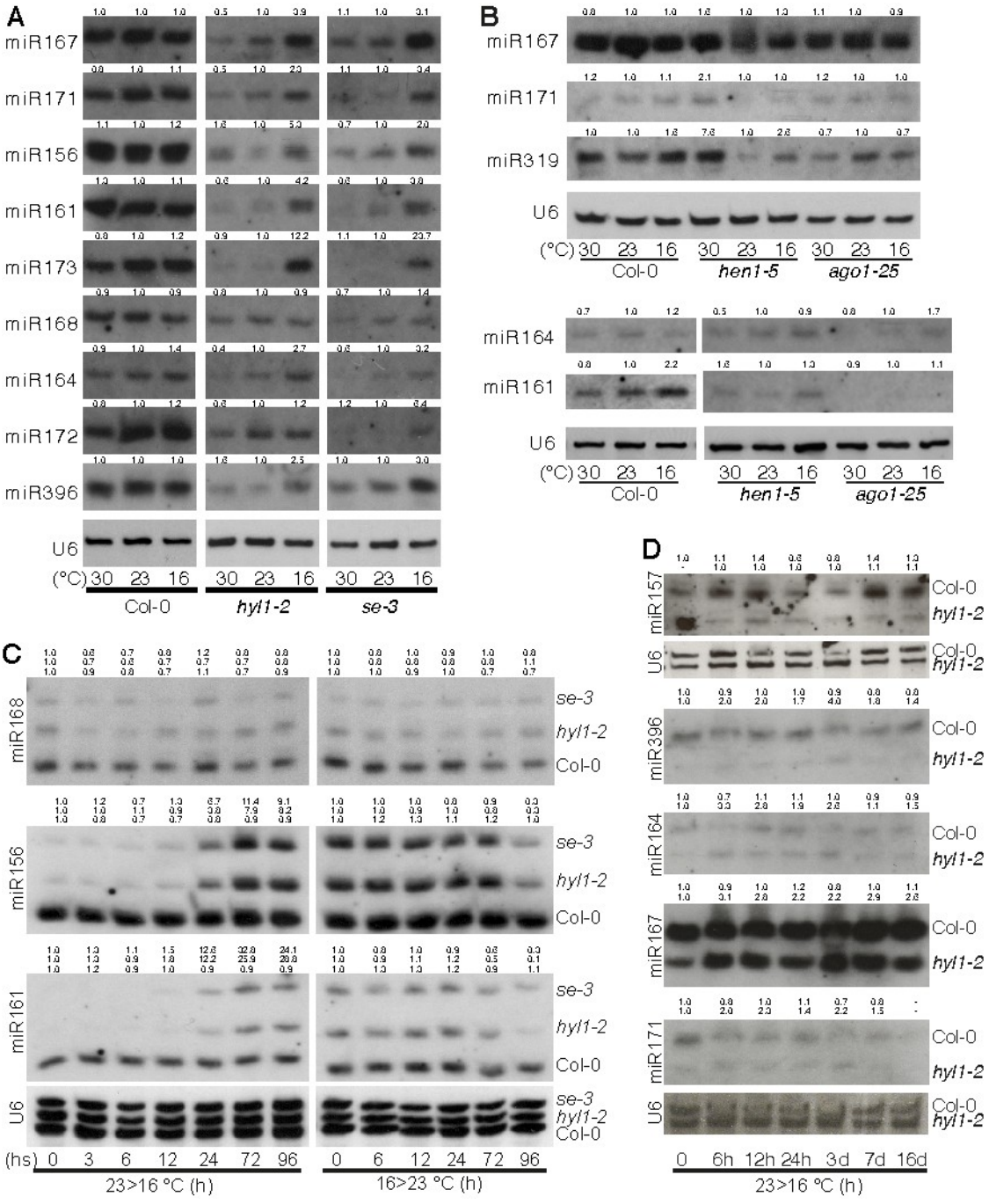

Fig. 2. MiRNA production in mutants grown at different temperatures. (A) RNA blots for detecting miRNAs in Col-0, *hyl1-2* and *se-3* plants grown at different temperatures. U6 was used as a loading control. (B) RNA blots for detecting miRNAs in Col-0, *ago1-25* and *hen1-5* plants grown at different temperatures. U6 was used as a

loading control. (C) and (D) RNA blots for detecting miRNAs in Col-0, *hyl1-2* and *se-3* plants grown at 23 °C for 5 days and then transferred to 16 °C for a given period of time (left blots, D) or grown at 16 °C for 5 days and then transferred to 23 °C for a given period of time (right blots). U6 was used as a loading control. Samples from different mutants plants were loaded in the same gel with a 15 minutes interval to facilitate comparison. In all panels, signal intensity was calculated using ImageJ and expressed as relative to the samples at 23°C for each genotype (A and B) or to the time point 0 of each genotype (C and D).

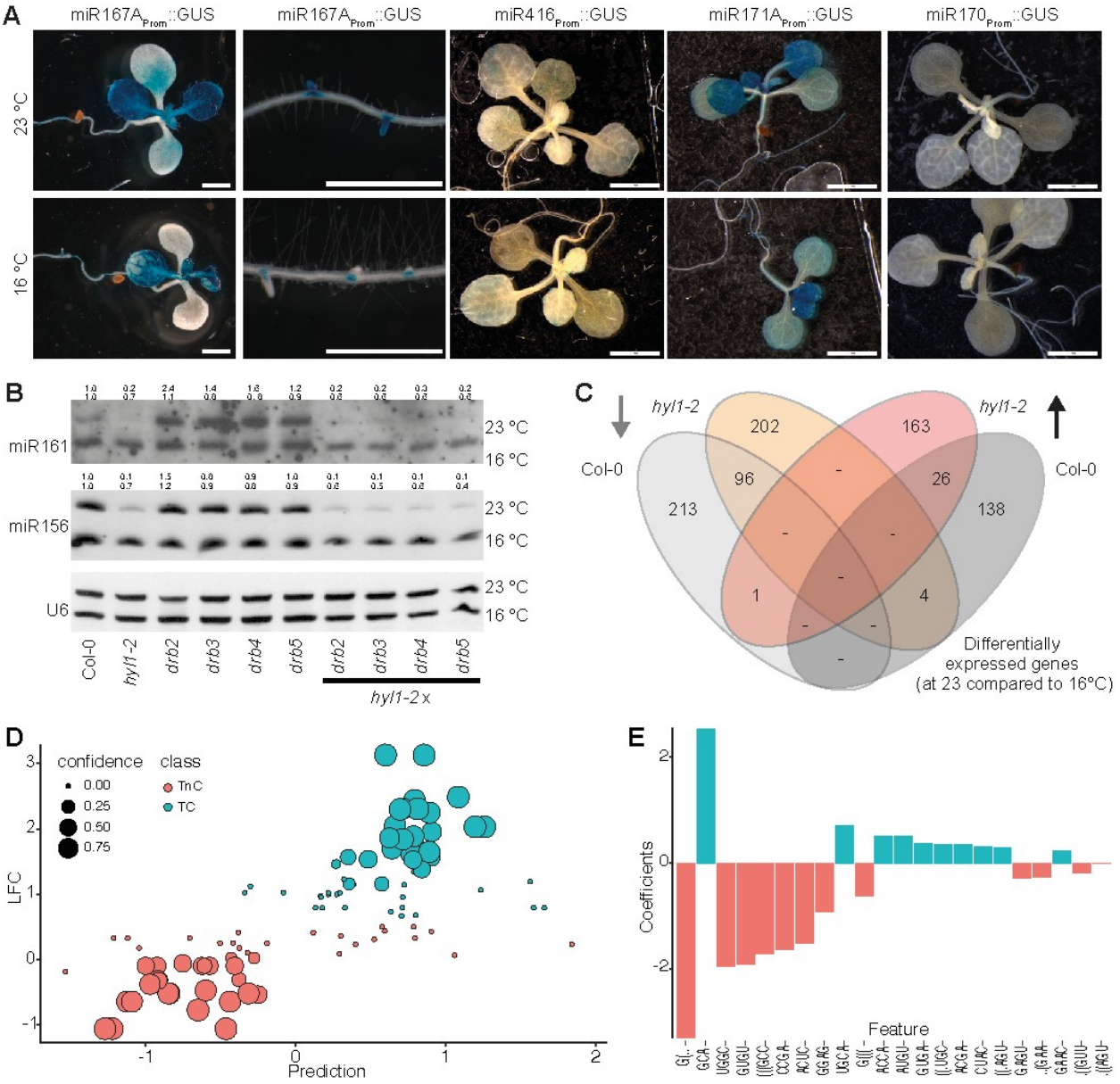

Fig. 3. MiRNA production recovery at 16 °C in *hyl1-2* is probably not due to a redundant factor but to pri-miRNA secondary structure. (A) Histochemical staining for activity of GUS miRNA-promoter reporters of transgenic plants grown at 23 °C and then transferred, or not, for 6 days, to 16 °C. Scale bars represent 1 cm. (B) RNA blots for detecting miRNAs in Col-0, *hyl1-2, drb2* to *drb5* single or *drb2* to *drb5/hyl1-2* double mutants grown at different temperatures. U6 was used as a loading control. Samples extracted from plants grown at 23 or 16 °C were loaded in the same gel with a 15 minutes interval to facilitate comparison. Signal intensity was calculated using ImageJ and expressed as relative to the Col-0 sample for each genotype. (C) Venn diagram showing genes differentially expressed in Col-0 and *hyl1-2* plants grown at 23 compared to 16 °C. Light orange (*hyl1-2)* and grey (Col-0) balloons show genes that are down-regulated, red (*hyl1-2*) and black (Col-0) balloons show genes that are up-regulated at 23 °C relative to 16°C. (D) Groups of sequences separated according to log2 fold change (LFC) into two groups: miRNAs with accumulation levels changing with temperature (TC) and not changing with temperature (TnC). Each circle represents a sequence, colored according to its corresponding group: TC in green and TnC in red. The size of each circle indicates its corresponding confidence level. (E) Features selected by LASSO. Positive LASSO coefficient for the feature indicates that it is important for the group TC (green), while a negative coefficient indicates that the feature is important for the TnC (red) group.

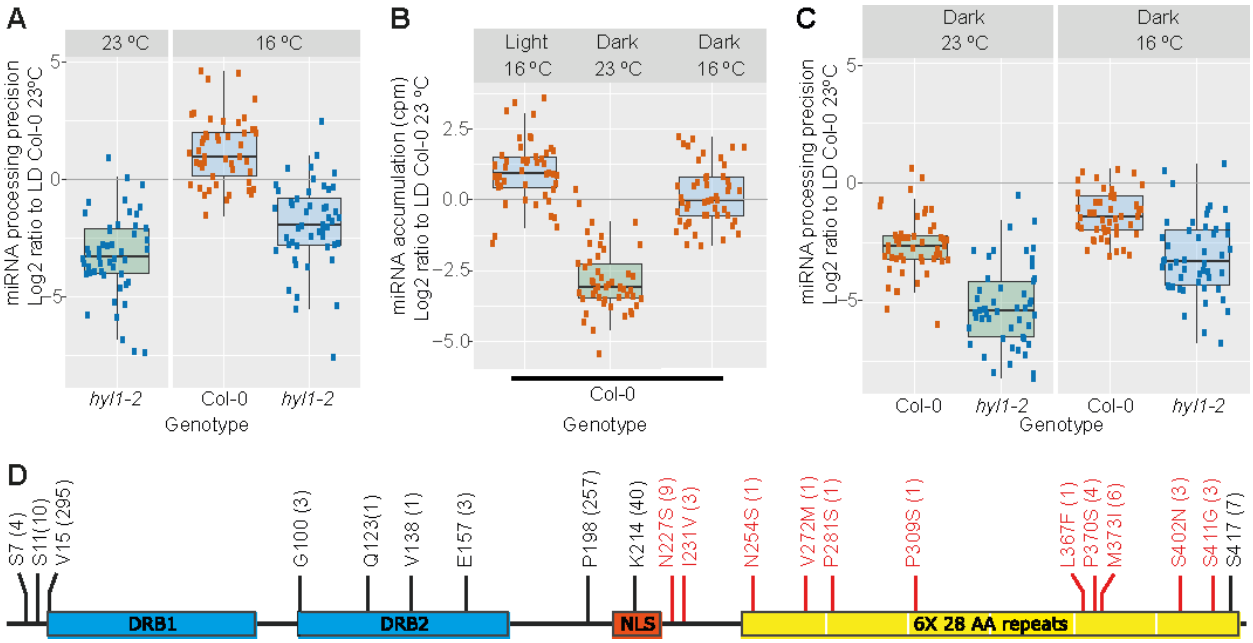

Fig. 4. A temperature drop improves miRNA processing precision. (A and C) Precisely processed miRNA reads at all highly expressed *MIRNA* loci (see (Liu et al. 2012)). Each dot represents an individual miRNA, while black bars indicate medians. MiRNA levels in all samples are expressed as a ratio to the precisely processed miRNAs in Col-0 plants grown at 23 °C in LD photoperiod. (B) Normalized small RNA mapped to mature miRNAs expressed as counts per million (cpm). MiRNA accumulation is shown as the ratio to the levels in Col-0 plants grown at 23 °C in LD photoperiod. Each dot represents an individual miRNA while black bars indicate medians. (D) Polymorphisms detected in the *HYL1* coding sequence among 309 *Arabidopsis thaliana* natural accessions analyzed. Blue boxes represent HYL1 double strand RNA Binding Domains (DRB), the orange box shows the nuclear localization signal (NLS), and yellow boxes represent the C-terminal six times repeated 28 amino acid sequence. Black lines indicate polymorphisms causing synonymous mutations. Red lines indicate polymorphisms causing non-synonymous mutations. Amino acid, position, and substitution are given in one letter amino acid code. In all cases, the number of accessions presenting a polymorphism is given in parenthesis over a total of 309 that had sequence information for all analyzed HYL1 polymorphisms.